https://ntrs.nasa.gov/search.jsp?R=20180002158 2018-07-23T13:30:10+00:00Z

NASA/TM–2018–219876

Spectral mass gauging of unsettled liquid with acoustic waves

Jeffrey Feller
NASA Ames Research Center, Moffet Field, CA, 94035

Ali Kashani
MEI Company, NASA Ames Research Center, Moffett Field, CA, 94035

Michael Khasin
SGT, Inc., NASA Ames Research Center, Moffett Field, CA, 94035

Cyrill Muratov
Department of Mathematical Sciences, NJIT, Newark, NJ, 07102

Viatcheslav Osipov
Hardware Physics LLC, Redding, CA, 96001

Surendra Sharma
NASA Ames Research Center, Moffet Field, CA, 94035

January 2018

NASA STI Program ... in Profile

Since its founding, NASA has been dedicated to the advancement of aeronautics and space science. The NASA scientific and technical information (STI) program plays a key part in helping NASA maintain this important role.

The NASA STI Program operates under the auspices of the Agency Chief Information Officer. It collects, organizes, provides for archiving, and disseminates NASA's STI. The NASA STI Program provides access to the NASA Aeronautics and Space Database and its public interface, the NASA Technical Report Server, thus providing one of the largest collection of aeronautical and space science STI in the world. Results are published in both non-NASA channels and by NASA in the NASA STI Report Series, which includes the following report types:

- TECHNICAL PUBLICATION. Reports of completed research or a major significant phase of research that present the results of NASA programs and include extensive data or theoretical analysis. Includes compilations of significant scientific and technical data and information deemed to be of continuing reference value. NASA counterpart of peer-reviewed formal professional papers, but having less stringent limitations on manuscript length and extent of graphic presentations.
- TECHNICAL MEMORANDUM. Scientific and technical findings that are preliminary or of specialized interest, e.g., quick release reports, working papers, and bibliographies that contain minimal annotation. Does not contain extensive analysis.
- CONTRACTOR REPORT. Scientific and technical findings by NASA-sponsored contractors and grantees.
- CONFERENCE PUBLICATION. Collected papers from scientific and technical conferences, symposia, seminars, or other meetings sponsored or co-sponsored by NASA.
- SPECIAL PUBLICATION. Scientific, technical, or historical information from NASA programs, projects, and missions, often concerned with subjects having substantial public interest.
- TECHNICAL TRANSLATION. English-language translations of foreign scientific and technical material pertinent to NASA's mission.

Specialized services also include creating custom thesauri, building customized databases, and organizing and publishing research results.

For more information about the NASA STI Program, see the following:

- Access the NASA STI program home page at `http://www.sti.nasa.gov`
- E-mail your question via the Internet to `help@sti.nasa.gov`
- Fax your question to the NASA STI Help Desk at (443) 757-5803
- Phone the NASA STI Help Desk at (443) 757-5802
- Write to
  NASA STI Help Desk
  NASA Center for AeroSpace Information
  7115 Standard Drive
  Hanover, MD 21076–1320

NASA/TM–2018–219876

Spectral mass gauging of unsettled liquid with acoustic waves

Jeffrey Feller
NASA Ames Research Center, Moffet Field, CA, 94035

Ali Kashani
MEI Company, NASA Ames Research Center, Moffett Field, CA, 94035

Michael Khasin
SGT, Inc., NASA Ames Research Center, Moffett Field, CA, 94035

Cyrill Muratov
Department of Mathematical Sciences, NJIT, Newark, NJ, 07102

Viatcheslav Osipov
Hardware Physics LLC, Redding, CA, 96001

Surendra Sharma
NASA Ames Research Center, Moffet Field, CA, 94035

National Aeronautics and
Space Administration

Ames Research Center, Moffett Field, CA, 94035-0001

January 2018

The use of trademarks or names of manufacturers in this report is for accurate reporting and does not constitute an offical endorsement, either expressed or implied, of such products or manufacturers by the National Aeronautics and Space Administration.

Available from:

NASA Center for AeroSpace Information
7115 Standard Drive
Hanover, MD 21076-1320
(443) 757-5802

Abstract

Propellant mass gauging is one of the key technologies required to enable the next step in NASA's space exploration program. At present, there is no reliable method to accurately measure the amount of unsettled liquid propellant of an unknown configuration in a propellant tank in micro- or zero gravity. We propose a new approach to use sound waves to probe the resonance frequencies of the two-phase liquid-gas mixture and take advantage of the mathematical properties of the high frequency spectral asymptotics to determine the volume fraction of the tank filled with liquid. We report the current progress in exploring the feasibility of this approach, both experimental and theoretical. Excitation and detection procedures using solenoids for excitation and both hydrophones and accelerometers for detection have been developed. A $\sim 3\%$ uncertainty for mass-gauging was demonstrated for a 200-liter tank partially filled with water for various unsettled configurations, such as tilts and artificial ullages. A new theoretical formula for the counting function associated with axially symmetric modes was derived. Scaling analysis of the approach has been performed to predict an adequate performance for in-space applications.

1 Introduction

The ability to quickly and accurately gauge the amount of the available propellant in a large-scale cryogenic propellant tank is one of the basic requirements to a successful tank design [1]. Under settled conditions, a wide range of mass gauging techniques are available [2]. These techniques usually work by determining the location of the liquid/gas interface in the tank with the help of, e.g., wet/dry sensors, and using it to infer the liquid propellant volume from the knowledge of the tank geometry. However, propellant mass gauging becomes a significant challenge under microgravity conditions, since in this case both the location and the shape of the ullage are a priori unknown. Boiling of cryogenic propellants near localized heat leaks and the formation of multiphase liquid-vapor foam adds further uncertainties to the liquid/vapor volume ratio [3]. Currently, there is no technological solution that is capable of determining the volume of unsettled liquid propellant of an unknown configuration in a large-scale cryogenic tank to within a few per cent uncertainty. In addition, even under settled conditions, propellant sloshing may add a significant degree of uncertainty to the volume measurements.

Propellant mass gauging techniques have been the subject of intense research since the 1960s (for a review, see [2]). At present, several advanced techniques for propellant mass gauging under reduced gravity conditions have been developed, including the reduced gravity Cryo Tracker system [4], Fiber Optic Sensing system [5], radio frequency (RF) mass gauging technology [2, 6, 7], all of which require hardware installation inside the tank, and Modal Propellant Gauging technique [8, 9], which is essentially non-intrusive. In particular, the RF mass gauging technology has been especially promising for operating under reduced gravity conditions, since its principle of operation does not rely directly on sensing the propellant level in the tank. Instead, an antenna inside the tank excites various electromagnetic resonance modes in the partially filled tank. A proprietary pattern matching algorithm is then used to compare the measured resonance frequencies with a database of the eigenfrequencies computed under various assumptions about the liquid configurations. The best match thus obtained is used to predict the fill level. Related concepts, using the acoustic resonance modes instead, were also proposed in the past [10] and recently in the Modal Propellant Gauging approach [8, 9]. The RF mass gauging technique was demonstrated to perform well (to within 2% uncertainty) under fully settled conditions and is currently considered among the best to operate under microgravity conditions in large-scale propellant tanks [6]. At the same time, the results of low-g testing exhibited strong temporal variability, indicating a significant amount of sloshing and/or fluid motion driven by capillary forces. As a consequence, the inferred fill level oscillated wildly, essentially precluding a possibility of an accurate fill level measurement.

The differences between the settled vs. unsettled RF mass gauging

performance should not be surprising, since there exists a fundamental mathematical difficulty in using spectral information alone to characterize the properties of heterogeneous wave-carrying media [11, 12]. As the data matching algorithm determines not only the closest fill level, but also the associated propellant configuration that fits best the measured spectral data, the algorithm should in principle be capable of determining the propellant configuration in the tank. However, it is known that this inverse problem is severely ill-posed, since identical spectral data may come from very different spatial domains (for an explicit counterexample, see [13]). In particular, any kind of regularization of the continuum model required to infer the shape of the propellant from the spectral data would also suffer from strong sensitivity to noise. As a consequence, for small but fixed amount of noise the pattern-matching performance would be expected to degrade above a certain noise-dependent level of spatial resolution. This may impose intrinsic limits on the accuracy of pattern-matching approaches in general, even when measurements can be done very accurately. We note that the foregoing arguments do not preclude successful pattern-matching for special classes of liquid configurations that can be parametrized by a small number of parameters. However, they raise serious concerns about the reliability of pattern-matching mass-gauging in the general case of a priori unknown propellant shapes in zero-gravity, when essentially random forces associated with the forced convection, Marangoni forces and surface tension prevail. In this situation a shape-blind methodology becomes indispensable.

In this paper we report our results on a mass-gauging approach which is intrinsically shape-blind as it is based on rigorously shape-invariant characteristics of acoustic spectra in the cavity of an unknown shape.

2 Spectral asymptotics for an acoustic cavity

In his famous mathematical work from 1911, H. Weyl proved that the high frequency asymptotics of the spectrum of the Laplacian in a three-dimensional spatial domain with Dirichlet boundary conditions depends on the domain only through its volume [16–18]. Ever since, Weyl's analysis has been greatly expanded and now provides rigorously justified asymptotic expansion formulas for the large eigenvalue asymptotics in the case of various differential operators and boundary conditions (for a recent review, see [19]). We note that sharp asymptotic expansion formulas for the eigenvalue problems involving heterogeneous media have been established only fairly recently and constitute a major advance in the mathematical analysis of partial differential equations [20].

Below we illustrate the Weyl's asymptotic formula arising from the studies of a propellant tank with thin walls filled with a heavy liquid propellant, such as liquid oxygen (LOx) or kerosine. Both the ullage and the propellant can be treated as acoustic cavities, with somewhat differ-

ent boundary conditions as explained below. Since boundary conditions for the ullage are more complex, ullage acoustic cavity will be considered first to illustrate the Weyl's formula in greater generality.

For simplicity, we assume that the ullage has the shape of a simply connected bounded domain $\Omega \subset \mathbb{R}^3$, partially in contact with the tank walls. The portion of the wall which is in contact with the ullage will be denoted by $\partial\Omega_-$, and the liquid/gas interface is denoted by $\partial\Omega_+$. The boundary of the ullage is the union of the gas/wall and gas/liquid surfaces: $\partial\Omega = \partial\Omega_- \cup \partial\Omega_+$.

To describe the acoustic eigenmodes in the ullage, we write the Helmholtz equation in the gas phase:

$$-c^2 \Delta p_l = (2\pi f_l)^2 p_l \qquad \text{in} \qquad \Omega. \tag{1}$$

Here p_l and f_l are the l-th pressure eigenfunction and eigenfrequency, respectively, Δ is the three-dimensional Laplacian, and c is the sound speed in the gas phase. To close this eigenvalue problem, we need to provide the boundary conditions satisfied by p_l at $\partial\Omega$. We point out that in general this would lead to a coupling between the acoustic modes in the ullage and those in the liquid and the tank walls (shell modes). However, when the impedance contrast between the liquid and gas phases is high, such as, for example, in LOx (sound speed $c = 181$ m/s and density $\rho = 6.9$ kg/m^3 for oxygen vapor at pressure $p_0 = 1.6$ atm vs. $c_L = 865$ m/s and $\rho_L = 1120$ kg/m^3 in the liquid phase at saturation, respectively), it is a very good approximation to assume a rigid wall boundary condition for the gas pressure at the liquid/gas interface $\partial\Omega_+$. Acoustically, this corresponds to zero velocity condition and, hence, zero normal derivative of the pressure boundary condition on $\partial\Omega_+$ [21]. At the same time, if the tank walls are sufficiently thin, it is reasonable to assume the pressure release boundary condition on $\partial\Omega_-$, which amounts to setting the acoustic pressure there to zero. The validity of this approximation depends on the details of the elastic properties of the pressurized tank walls and their associated shell modes (see, e.g., [22]). We will get back to this point later, but to get a rough idea of the validity of this approximation, one can compare the total mass of the gas in the ullage with that of the tank walls. For a cylindrical tank of radius $R = 2.5$ m and height $H = 4$ m, comparable in size to that of the LOx tank in the third stage of the Saturn V rocket [23], the gas mass exceeds that of the aluminum walls when the average wall thickness d_w falls below ~ 3 mm. For thinner walls, the pressure release boundary condition should, therefore, be reasonable. To summarize the above discussion, we impose the following boundary conditions on different portions of the boundary $\partial\Omega$:

$$\nu \cdot \nabla p_l|_{\partial\Omega_+} = 0, \qquad p_l|_{\partial\Omega_-} = 0, \tag{2}$$

which isolate the acoustic modes of the gas in the ullage from the rest of the system.

The spectral asymptotics of the eigenvalue problem in Eqs. (1) and (2) deals with the eigenfrequency counting function defined as

$$N(f) = \sum_{l=0}^{\infty} \theta(f - f_l), \tag{3}$$

where $\theta(x)$ is the Heaviside step function. Note that we have $f_l = c\sqrt{\lambda_l}/(2\pi)$, where λ_l are the eigenvalues of the Laplacian defined on the spatial domain occupied by the ullage with the corresponding boundary conditions. For this problem, Weyl conjectured [18], and several authors later proved [24,25] (for significant earlier works, see [26–29]; for reviews, see [11, 19]) that

$$N(f) = \frac{4\pi|\Omega|f^3}{3c^3} + \frac{\pi|\partial\Omega_+|f^2}{4c^2} - \frac{\pi|\partial\Omega_-|f^2}{4c^2} + o(f^2), \qquad f \to \infty, \tag{4}$$

where $|\Omega|$ is the volume of Ω and $|\partial\Omega_\pm|$ is the area of $\partial\Omega_\pm$. Observe that the leading order term in the above formula is proportional to the ullage volume and is *independent* of the ullage shape. Thus, measuring the eigenfrequency counting function $N(f)$ and fitting it to the functional form in Eq. (4) can in principle yield the ullage volume to arbitrary precision, provided the counting function is known accurately up to sufficiently high frequencies. It is important to note that even though the surface terms do depend on the unknown ullage shape, the knowledge of the shape is not required for the volume inference. Only the terms' (known) scaling with f matters.

We note that the counting function takes into account the multiplicity of the eigenfrequencies. Therefore, in the presence of degeneracies the counting function obtained experimentally will be underestimated. Yet, it is expected that in the absence of symmetries all eigenfrequencies should be generically non-degenerate. To break the degeneracy in the case of, e.g., axially symmetric propellant tanks, one would, therefore, need to introduce heterogeneities, such as baffles, into the tank.

The asymptotic formula in Eq. (4) forms the basis of our mass gauging approach. Its utility will now be evaluated for a number of typical propellant tank geometries for which the spectra can be derived in closed form analytically. We note that for general ullage geometries and mixed Dirichlet-Neumann boundary conditions as in Eq. (2), solving the acoustic eigenvalue problem, also known as the Zaremba eigenvalue problem, is a significant challenge, both analytically and numerically (for some recent progress, see [30]). We postpone the studies of more general unsettled ullage geometries to future work.

In addition to using the formula in Eq. (4), we will also take advantage of its two-dimensional analog for the problem posed in $\Omega_0 \subset \mathbb{R}^2$ [19]:

$$N_0(f) = \frac{\pi|\Omega_0|f^2}{c^2} + \frac{|\partial\Omega_0^+|f}{2c} - \frac{|\partial\Omega_0^-|f}{2c} + o(f), \qquad f \to \infty. \tag{5}$$

where $\partial\Omega_0^{\pm}$ are the portions of the boundary of Ω_0 on which Neumann and Dirichlet boundary conditions are prescribed, respectively, $|\Omega_0|$ is the area of Ω_0 and $|\partial\Omega_0^{\pm}|$ are the perimeters of $\partial\Omega_0^{\pm}$.

3 Analysis of the spectral asymptotics for the cylindrical geometry

3.1 Acoustic eigenfrequencies

3.1.1 Ullage modes

We begin by considering a cylindrical ullage of radius R and height H, with the gas in contact with the liquid at the settled bottom horizontal surface. In cylindrical coordinates, the eigenvalue problem in Eq. (1) can be written as

$$-\frac{1}{r}\frac{\partial}{\partial r}\left(r\frac{\partial p_l}{\partial r}\right)-\frac{1}{r^2}\frac{\partial^2 p_l}{\partial\varphi^2}-\frac{\partial^2 p_l}{\partial z^2}=\left(\frac{2\pi f_l}{c}\right)^2 p_l, \tag{6}$$

where $p_l = p_l(r,\varphi,z)$ is specified in the domain

$$\Omega=\{(r,\varphi,z)\ :\ 0<r<R,\ 0\le\varphi\le 2\pi,\ 0<z<H\}. \tag{7}$$

with boundary conditions

$$\left.\frac{\partial p_l}{\partial z}\right|_{z=0}=0,\quad p_l|_{z=H}=p_l|_{r=R}=0, \tag{8}$$

$$\left.\frac{\partial p_l}{\partial\varphi}\right|_{\varphi=0}=\left.\frac{\partial p_l}{\partial\varphi}\right|_{\varphi=2\pi},\quad p_l|_{\varphi=0}=p_l|_{\varphi=2\pi}. \tag{9}$$

This problem admits an explicit solution:

$$p_{kmn}(r,\varphi,z)=J_m(a_{mn}r/R)e^{im\varphi}\cos\left(\frac{\pi(2k+1)z}{2H}\right), \tag{10}$$

where $J_m(x)$ is the Bessel function of order m of the first kind, a_{mn} is the n-th zero of $J_m(x)$, now indexed by $m=0,\pm1,\pm2,\ldots$, $n=1,2,\ldots$, and $k=0,1,2,\ldots$. The corresponding eigenfrequencies are

$$f_{kmn}=\frac{c}{2\pi}\sqrt{\frac{\pi^2(2k+1)^2}{4H^2}+\frac{a_{mn}^2}{R^2}}. \tag{11}$$

Defining the eigenfrequency counting function

$$N(f)=\sum_{n=1}^{\infty}\sum_{m=-\infty}^{\infty}\sum_{k=0}^{\infty}\theta(f-f_{kmn}), \tag{12}$$

we then write the expression for Weyl's asymptotic formula from Eq. (4):

$$N(f)=\frac{4\pi^2R^2Hf^3}{3c^3}-\frac{\pi^2RHf^2}{2c^2}+o(f^2),\qquad f\to\infty. \tag{13}$$

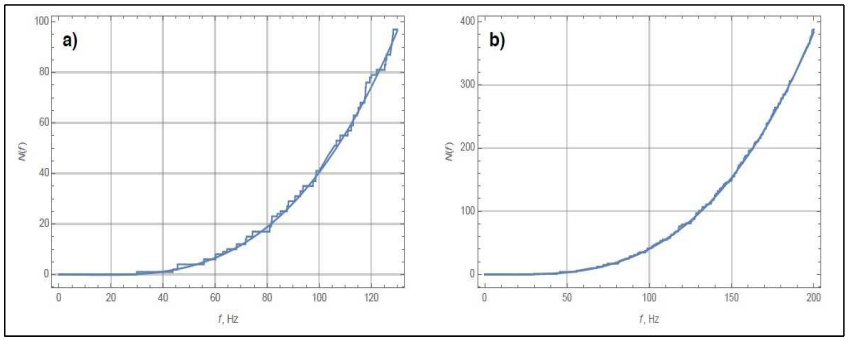

Figure 1. The eigenfrequency counting function for the spectral problem in Eq. (6) and Eq. (8) and the corresponding predictions of Weyl's asymptotic formula. In both (a) and (b), the broken line shows the exact eigenfrequency counting function, and the solid line shows the result from Eq. (13). In (a), the first 100 eigenfrequencies are shown. In (b), the first 400 eigenfrequencies are shown.

Choosing $R = 2.5$ m, $H = 4$ m and $c = 181$ m/s, corresponding to a LOx tank mentioned above, we obtain the theoretical eigenfrequency counting function shown in Fig. 1. One can see an excellent agreement between $N(f)$ from the exact definition in Eq. (3) with f_l given by Eq. (11) and the asymptotic prediction in Eq. (13), for the frequency range yielding the first 100 eigenfrequencies (Fig. 1a) and the first 400 eigenfrequencies (Fig. 1b), respectively.

3.1.2 Liquid modes

Modes in the propellant can be calculated similarly to the ullage modes above, from Eq.(6) using modified boundary conditions, to account for the pressure release condition all over the boundary. Assuming propellant resides in the domain

$$\Omega = \{(r, \varphi, z) \ : \ 0 < r < R, \ 0 \leq \varphi \leq 2\pi, \ 0 < z < H\}. \tag{14}$$

we impose the following boundary conditions

$$p_l|_{z=0} = p_l|_{z=H} = p_l|_{r=R} = 0, \tag{15}$$

$$p_l|_{\varphi=0} = p_l|_{\varphi=2\pi}, \quad \left.\frac{\partial p_l}{\partial \varphi}\right|_{\varphi=0} = \left.\frac{\partial p_l}{\partial \varphi}\right|_{\varphi=2\pi}, \tag{16}$$

as expected on physical grounds. Indeed, in contrast to ullage, the pressure release boundary condition must be imposed not only on the thin wall of the tank but on the liquid/gas interface as well.

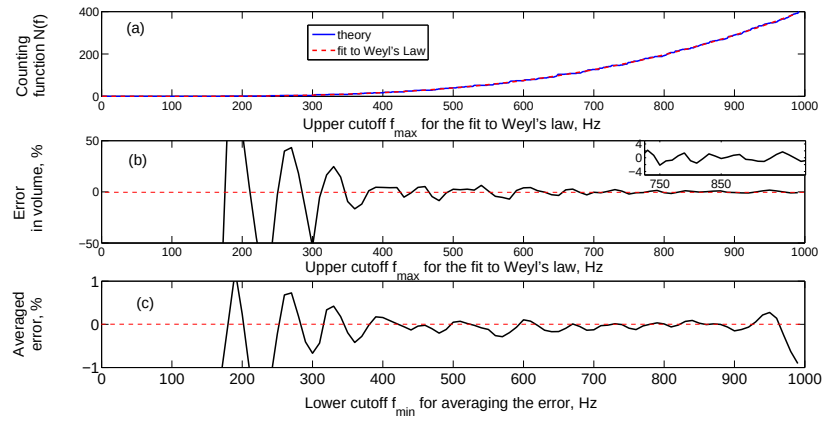

Figure 2. Model calculations: (a) Counting function for a cylindrical tank, $IR = 2.5m$, $H = 4m$ filled with LOx; (b)Error in inferred volume as a function of the cutoff frequency; (c) Averaged error (see the main text for the definition) in the range between a lower and upper cutoff $f_{max} = 1kHz$ as a function of the lower cutoff. Error is seen to be $< 2\%$ for $N > 300$. Averaged error is $< 0.3\%$. .

This problem admits an explicit solution:

$$p_{kmn}(r, \varphi, z) = J_m(a_{mn} r/R) e^{im\varphi} \sin\left(\frac{\pi k z}{H}\right), \tag{17}$$

where $J_m(x)$ is the Bessel function of order m of the first kind, a_{mn} is the n-th zero of $J_m(x)$, now indexed by $m = 0, \pm 1, \pm 2, \ldots$, $n = 1, 2, \ldots$, and $k = 1, 2, \ldots$. The corresponding eigenfrequencies are

$$f_{kmn} = \frac{c}{2\pi} \sqrt{\left(\frac{\pi k}{H}\right)^2 + \frac{a_{mn}^2}{R^2}}. \tag{18}$$

and the expression for Weyl's asymptotic formula from Eq. (4) becomes:

$$N(f) = \frac{4\pi^2 R^2 H f^3}{3c^3} - \frac{\pi^2 R^2}{2c^2}\left(1 + \frac{H}{R}\right) f^2 + o(f^2), \qquad f \to \infty. \tag{19}$$

Choosing $R = 2.5$ m, $H = 4$ m and $c = 181$ m/s, as previously, we obtain the theoretical eigenfrequency counting function shown in Fig. 2 (a). Again, one can see an excellent agreement between $N(f)$ from the exact definition in Eq. (3) with f_l given by Eq. (18) (red dashed line) and the asymptotic prediction in Eq. (19) (blue line), for the frequency range yielding the first 400 eigenfrequencies.

3.2 Comparison with Weyl's asymptotics

Here we discuss the accuracy of the approximation in more details. Coming back to Figure 2, in panel (b) we see the relative error in the volume

inference as a function of the cut-off frequency f_{max} oscillates around zero as f_{max} increases and tends to zero. The error is calculated as $\varepsilon = (V_w - V)/V \cdot 100\%$, where V is the actual volume of the propellant $V = \pi R^2 H$ and V_w is the value inferred using the best fit to Weyl's formula. The error is seen to fall below 3% for $N(f_{max}) > 400$. Oscillations of the error with the cut-off frequency seem to be a generic feature of the convergence and are observed in other geometries (boxes, spheres) and boundary conditions (Neumann, i.e., a rigid wall). This gives an idea that averaging of the inferred volume over the oscillations may accelerate its convergence to the actual value. Figure 2 (c) displays the result of such an averaging. The *averaged error* is obtained by integration of the error $\varepsilon(f)$ over the interval $[f_{min}, f_{max}]$ for fixed f_{max} and varying f_{min} and can be considered a function of f_{min}. Indeed, the averaged error fall below 0.3% for $N > 200$.

We are not aware of rigorous results regarding the convergence properties of the Weyl's formula with the cut-off frequency. The convergence is expected and empirically found to depend on boundary conditions (Dirichelet boundary conditions are found to lead to faster convergence of the error with N than Neumann boundary conditions), and for given boundary conditions it is expected to depend on the shape of the cavity, propellant or ullage. Some intuition for the latter can be gained considering cylindrical geometry. On dimensional grounds it is clear that $N = F(\varepsilon, H/R)$, where N is the mode counting number corresponding to the error ε, H the height and R the radius of the domain. It is important to note that N is independent of the fluid properties, e.g., the speed of sound. Function F will depend on boundary conditions. For given boundary conditions and error ε it can be expected that N increases as $H/R \to 0$ or $H/R \to \infty$. Indeed, in these limits the domain becomes quasi-$2D$ and quasi-$1D$, respectively. Therefore, one has to go to higher count number to account for the vanishing dimension. Numerical experiments displayed in Figure 3 and Eq.(19) imply that asymptotic dependence at $H/R \to 0$ becomes $N = (R/H)^2 F_1(\varepsilon)$ and asymptotic dependence at $H/R \to \infty$ becomes $N = (H/R) F_2(\varepsilon)$, where $F_1 \sim F_2$.

One practical conclusion from these observations is that for a given relative uncertainty much more liquid modes must be counted as the filling level of the tank decreases significantly below the level where $R \lesssim H$. It should be noted, however, that the accuracy of propellant volume gauging is normally defined with respect to the full volume of the tank, therefore, lesser relative accuracy is required.

3.3 Peaks resolution

If the number of resolvable peaks were unlimited, one could arrive at arbitrarily small error in volume with the mode counting technique. In reality the resolution is limited by the dissipation and other factors such as temperature inhomogeneity of the fluid. The contribution of the latter

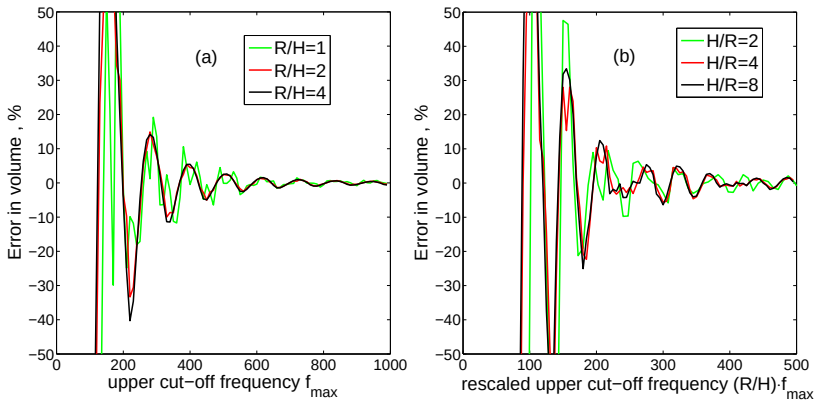

Figure 3. Model calculations: (a) Error in inferred volume as a function of the cutoff frequency f_{max} for the cylindrical cavity aspect ratios $R/H = 1, 2, 4, 8$. Based on (19) and the general scaling relation $N = F(\varepsilon, H/R)$ the calculation implies $\varepsilon = G(N(f_{max})(H/R)^2)$, leading to the $N = (R/H)^2 F_1(\varepsilon)$ asymptotic relation for $R/H \gg 1$. (b) Error in inferred volume as a function of the rescaled cutoff frequency $(R/H)\cdot f_{max}$ for aspect ratios $H/R = 2, 4, 8$. Based on (19) and the general scaling relation $N = F(\varepsilon, H/R)$ the calculation implies $\varepsilon = G(N(f_{max})R/H)$, leading to the $N = (H/R)F_2(\varepsilon)$ asymptotic relation for $H/R \gg 1$.

factor depends on the specific situation, is negligible close to thermal equilibrium and is not considered here. The tests reported below were performed under conditions very close to thermal equilibrium, where the effect of inhomogeneity was small. The dissipation of the acoustic waves occurs both in the bulk of the liquid or gas and in the boundary layer near the wall. The bulk contribution is generally negligible and the boundary layer dissipation will determine the available resolution in thermal equilibrium.

Formally, the peaks can be resolved provided their width 2Γ is smaller than the average peaks separation distance Δf near the cut-off frequency f corresponding to the given counting number $N(f)$:

$$\frac{2\Gamma}{2\pi\Delta f} \ll 1. \tag{20}$$

The average peaks separation around f can be estimated from Weyls law for:

$$\Delta f \approx \left(\frac{dN}{df}\right)^{-1} = \frac{f}{3N}; \quad f \approx \left(\frac{3c^3 N}{4\pi V}\right)^{1/3}. \tag{21}$$

Assuming the main source of dissipation is thermal boundary layer, the width of the peaks 2Γ can be estimated [21] for a domain (ullage or

propellant) of characteristic linear dimension $L \sim V^{1/3}$:

$$2\Gamma \approx \sqrt{\frac{4\pi f}{L^2}} \left[\sqrt{\nu} + \sqrt{\chi} \left(\frac{c_p}{c_v} - 1 \right) \right], \tag{22}$$

where μ is the kinematic viscosity, $\chi = \kappa/(\rho c_p)$ is the thermal diffusivity, κ is the thermal conductivity, c_p is the isobaric heat capacity and c_v is isochoric heat capacity of the gas or liquid. From Eqs.(21-22) we obtain the following estimate:

$$\frac{2\Gamma}{2\pi\Delta f} \approx 3\sqrt{\frac{N^2}{\pi f L^2}} \left[\sqrt{\nu} + \sqrt{\chi} \left(\frac{c_p}{c_v} - 1 \right) \right] \tag{23}$$

$$\approx 2N^{5/6} \left[\sqrt{\frac{\nu}{cL}} + \sqrt{\frac{\chi}{cL}} \left(\frac{c_p}{c_v} - 1 \right) \right], \tag{24}$$

which shows that the relative width scales as $L^{-1/2}$. From Eqs.(23) and (20) we obtain the following condition for the resolution, expressed in terms of the maximal number of peaks N_{max} resolved for the given tank and fluid properties:

$$N \ll N_{max} \equiv \left[\sqrt{\frac{\nu}{cL}} + \sqrt{\frac{\chi}{cL}} \left(\frac{c_p}{c_v} - 1 \right) \right]^{-6/5}. \tag{25}$$

Similar calculations show that the relative width contribution from bulk dissipation scales as L^{-1} and that generally $N_{max}|_{bulk} \sim (N_{max}|_{boundary})^{3/2}$, justifying neglecting the bulk dissipation.

In the previous subsection we saw that N determines the error in volume inference for the given fluid shape and boundary conditions. Therefore, Eq.(25) implies that the resolved N will increase and the error will decrease with the characteristic size of the tank L for similar shapes, fluid properties and boundary conditions. In addition, we expect that due to significantly lower dimensionless numbers $\nu/(cL)$ and $\chi/(cL)$ in liquids compared to gases higher resolution N can generally be achieved in gauging liquids. For oxygen at saturation temperature at $p = 1.6atm$, and for a tank of $L = 1m$ we find:

$$GOx: \ \sqrt{\frac{\nu}{cL}} = 7.7 \cdot 10^{-5}; \ \sqrt{\frac{\chi}{cL}} \left(\frac{c_p}{c_v} - 1 \right) = 3.9 \cdot 10^{-5};$$
$$N_{max} = 5.2 \cdot 10^4; \tag{26}$$
$$LOx: \ \sqrt{\frac{\nu}{cL}} = 1.2 \cdot 10^{-5}; \ \sqrt{\frac{\chi}{cL}} \left(\frac{c_p}{c_v} - 1 \right) = 7.9 \cdot 10^{-6};$$
$$N_{max} = 4.3 \cdot 10^5. \tag{27}$$

These observations imply that liquid modes counting will generally lead to a more accurate volume inference than the ullage modes counting.

3.4 Shell modes

We now go back to evaluating the effect of the shell modes on the spectral asymptotics of the acoustic eigenfrequencies. For a pressurized cylinder their spectrum had been worked out in [22] (assuming the top and bottom surfaces are clamped). The acoustic eigenfrequencies in the absence of coupling between the gas and the shell modes is given by

$$\begin{aligned} f_{km}^{shell} &= \frac{1}{2\pi}\left(\frac{k^2\pi^2}{H^2}+\frac{m^2}{R^2}\right) \\ &\times \sqrt{\frac{Ed_w^2}{12\rho_w(1-\sigma^2)}\left(1+\frac{12pR(1-\sigma^2)}{Ed_w^3[(m/R)^2+(k\pi/H)^2]}\right)}, \end{aligned} \tag{28}$$

where E is the Young modulus of the wall material, σ is its Poisson ratio, ρ_w is the wall mass density, d_w is the wall thickness, p is pressure inside the tank (assuming vacuum on the outside), $k = 1, 2, \ldots$ and $m = 0, \pm 1, \pm 2, \ldots$. Similarly to the case of the ullage, we define the eigenfrequency counting function $N^{shell}(f)$ associated with the shell modes. In Eq. (28), we took into account that at low frequencies the shell spectrum is dominated by the bending modes. Indeed, for compression modes the frequency f_{comp} would satisfy $f_{comp} \gtrsim c_w/H$, where $c_w = \sqrt{E/\rho_w}$ is the sound speed in the tank wall. Therefore, for aluminum, we have $c_w/H \simeq 1.3$ kHz, which greatly exceeds the acoustic frequencies of the ullage.

We note that the high frequency asymptotics of the eigenfrequencies f_{km}^{shell} is dominated by pure bending modes, for which

$$f_{km}^{shell} \simeq \frac{1}{2\pi}\left(\frac{k^2\pi^2}{H^2}+\frac{m^2}{R^2}\right)\sqrt{\frac{Ed_w^2}{12\rho_w(1-\sigma^2)}}, \qquad f \to \infty. \tag{29}$$

It is easy to see from this expression that $N^{shell}(f) \sim f$ as $f \to \infty$, so the presence of these modes does not affect the leading order asymptotics in Eq. (13) (Eq. (19)), if one counts both the ullage (propellant) and the shell modes. Nevertheless, one should take into consideration the late onset of the asymptotic behavior of N^{shell} for the shell modes under pressurization, which, according to Eq. (28), occurs only when $f \gtrsim f_0^{shell}$, where $f_0^{shell} = pR/\sqrt{E\rho_w d_w^4} \simeq 3$ kHz for the considered parameters. In the frequency range of interest, the shell modes are dominated by the membrane elasticity of the pressurized walls, yielding with very good accuracy

$$f_{km}^{shell} \simeq \frac{1}{2\pi}\sqrt{\frac{pR}{\rho_w d_w}\left(\frac{k^2\pi^2}{H^2}+\frac{m^2}{R^2}\right)}. \tag{30}$$

From this formula, it is not difficult to obtain that

$$N^{shell}(f) \simeq \frac{2\pi^2\rho_w d_w H f^2}{p}, \qquad f_1^{shell} \ll f \ll f_0^{shell}, \tag{31}$$

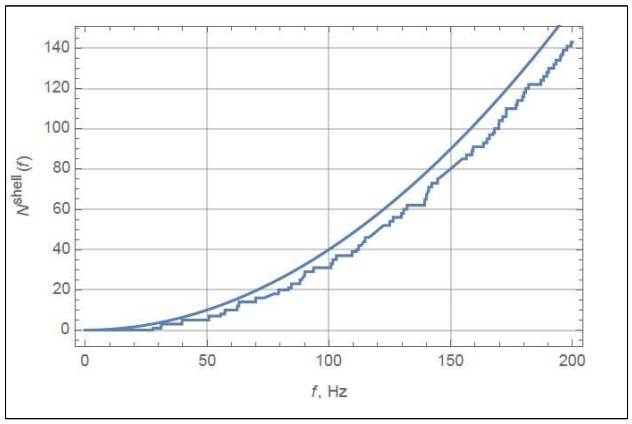

Figure 4. The eigenfrequency counting function for the shell modes obtained from Eq. (28) (broken line) and from Eq. (31) (solid line).

where $f_1^{shell} = \sqrt{pR/(4\rho_w d_w H^2)} \simeq 28$ Hz. This formula agrees well with the exact expression for $N^{shell}(f)$ from Eq. (28) in the frequency interval of interest (Fig. 4). We summarize the above observations by noting that the sum of the counting functions from the ullage (propellant) and from the shell modes still behaves as $N(f) \simeq Af^3 + Bf^2$, where the coefficient A is the same as in Eqs. (13) and Eq. (19). Therefore, the presence of the shell modes is not expected to alter the high frequency asymptotics of the ullage (propellant) modes, thus not precluding the ability to determine the ullage (propellant) volume with the mode counting approach.

4 Comparison with the experimental results in cylindrical geometries

4.1 Ullage modes counting tests

In this section we report results of the first series of experiments, where the ullage modes counting was performed. The aim was of measuring on the order of 100 acoustic eigenfrequencies, mostly in cylindrical tanks of various dimensions that were partially filled with water (settled at the bottom) and air at standard conditions (at the top). A PCB Piezotronics, Inc., impulse force hammer with a sensitivity of 2.458 mV/N was used to tap on the upper surface of the metallic tanks, and a PCB Piezotronics microphone with a sensitivity of 2.07 mV/Pa suspended inside the tank was used to acquire the acoustic signal. Data Physics Quattro was used for acoustic signal analysis, including standard FFT analysis, for frequencies up to 40 kHz at a sampling rate of 204.8 ksamples/sec. The impulse hammer was used in a transfer function mode where the microphone signal in Fourier space was divided by the signal from the hammer. The obtained data sets were provided for further data analysis to extract

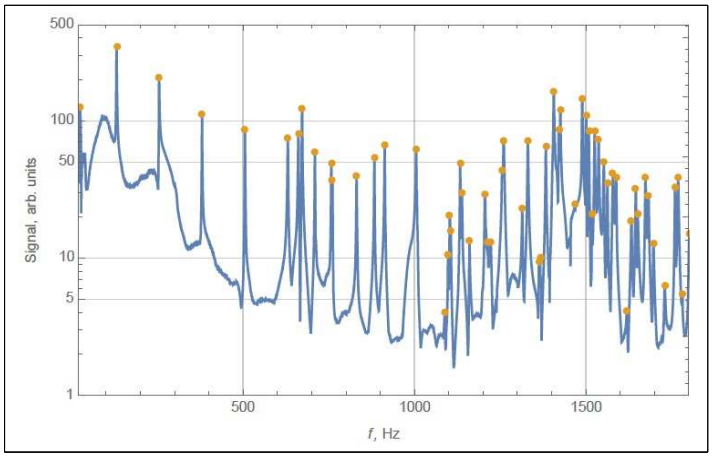

Figure 5. The acoustic signal from the tapping experiments (blue line) and the location of the peaks detected (gold points) for an empty large Dewar tank with radius $R = 15.24$ cm and height $H = 134.6$ cm.

the positions of the resonance peaks. In turn, we have developed an algorithm that allows to extract the peak locations from the measured data with the resolution of at least 10 Hz, which is comparable to the physical width of the measured peaks in the frequency domain. We then compared the observed spectra with their theoretical counterparts and used Weyl's asymptotic formula in Eq. (4) to predict the tank volume. Below we summarize the results of our analysis for several runs of the experiments.

We focus on a large Dewar tank in the form of a cylinder of radius $R = 15.2$ cm and height $H = 134.6$ cm. The choice of the Dewar is motivated by the fact that its evacuated double walls possess a higher degree of rigidity, decreasing the coupling of the cavity to the shell modes and to the exterior air. We take the sound speed to be that of dry air at standard conditions, $c = 343$ m/s. The obtained raw data and the frequency peaks detected in the frequency interval $0 \leq f \leq f_{max}$ with $f_{max} = 1.8$ kHz are shown in Fig. 5. The data consist of the upper envelope of 5 independent spectra obtained by tapping at different points on the tank lid. This maximizes the number of the modes detected by the microphone at a fixed location inside the tank close to the side wall. We then normalized the signal to its gaussian running average with the width of 1 kHz. The obtained spectrum was then processed by a peak finding routine, setting the smoothing parameter to 0.5 Hz and the threshold parameter to 0.0005 in order to reduce the number of parasitic peaks due to noise in the data. All the computations were done, using Mathematica 10.4 software. As can be seen from Fig. 5, this algorithm is capable of

detecting about 60 eigenfrequencies in the considered spectral interval.

In order to compare the results in Fig. 5 to the theoretical spectrum and apply Weyl's asymptotic formula, a number of modifications to the procedure described in Sec. 3 need to be introduced. First, for a tank with rigid walls, as is the case with the considered Dewar tank, the Dirichlet boundary condition should be replaced with Neumann, leading to the following expression for the eigenfrequencies:

$$f'_{kmn} = \frac{c}{2\pi}\sqrt{\frac{\pi^2 k^2}{H^2} + \frac{b_{mn}^2}{R^2}}, \tag{32}$$

where b_{mn} is the n-th zero of $J'_m(x)$, and we have $k = 0, 1, 2, \ldots$, $m = 0, \pm 1, \pm 2, \ldots$, and $n = 1, 2, \ldots$, with the convention that $b_{01} = 0$. Second, for each $m \neq 0$ the eigenfrequencies with the same value of $|m|$ coincide, making all non-axial eigenfrequencies doubly degenerate. With these observations, the asymptotic formula for the eigenfrequency counting function $N'(f)$ that does not count those degenerate eigenfrequencies:

$$N'(f) = \sum_{n=1}^{\infty}\sum_{m=0}^{\infty}\sum_{k=0}^{\infty}\theta(f - f'_{kmn}), \tag{33}$$

needs to be changed into

$$N'(f) = \frac{2\pi^2 R^2 H f^3}{3c^3} + \frac{\pi^2 R H f^2}{c^2} + o(f^2), \qquad f \to \infty. \tag{34}$$

A comparison between the theoretical eigenfrequency counting function (red), the one obtained from the data (blue) and the one from the Weyl's asymptotic formula (green) is presented in Fig. 6. One can see an excellent agreement between the measured spectrum and theory, down to individual peaks, in the entire interval $0 \leq f \leq f_{max}$. The agreement is quite remarkable and gives confidence in the ability to use the spectral asymptotics to predict the tank's volume. We also carried out our fitting procedure:

$$N'(f) \simeq A' f^3 + B' f^2, \tag{35}$$

with the obtained experimental data set to arrive at $A' = 4.45341 \times 10^{-9}$ s^3 and $B' = 0.0000103073$ s^2. Using the formula

$$V \simeq \frac{3c^3 A'}{2\pi} \tag{36}$$

then yields the value of V that is only 13% below the actual value. We note that the same procedure based on the theoretical spectrum produces the volume within 1.2% error. This, however, is somewhat fortuitous, since for Neumann boundary conditions the error of Weyl's asymptotics turns out to depend quite sensitively on the upper frequency cutoff f_{max}. For example, increasing the cutoff to $f_{max} = 3$ kHz in the theoretical

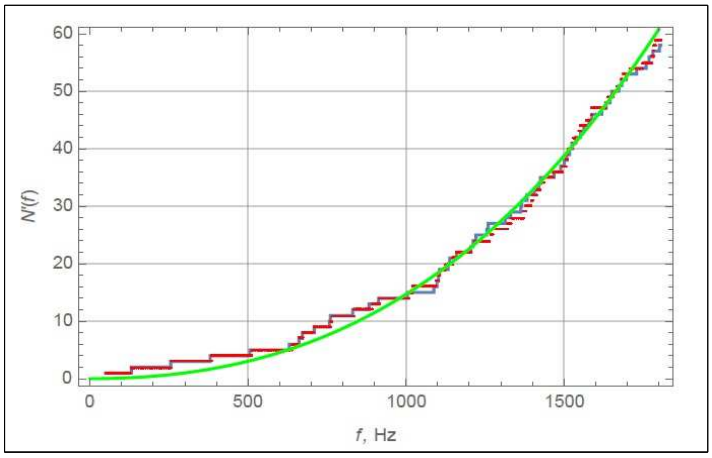

Figure 6. The eigenfrequency counting function $N'(f)$ obtained from theory (red), experimental data (blue) and Weyl's asymptotic formula (green) for the large Dewar tank in Fig. 5, with the cutoff frequency $f_{max} = 1.8$ kHz.

spectrum produces a theoretical prediction for V which is 11% below the actual value. Therefore, the accuracy of prediction obtained from the experimental data is close to the expected theoretical maximum at this value of the cutoff. The term *theoretical maximum* refers to the accuracy which would have been achieved if the entire acoustic spectrum were known exactly, i.e., if there were no measurement errors. The error in this case would have been due to the asymptotic nature of Weyls law and the finiteness of the cutoff frequency. We note that this somewhat lower accuracy of the asymptotic formula appears to be a feature of the Neumann problem and is absent from the Dirichlet problem considered in Sec. 3.1, which is good news for the application of the method to large-scale propellant tanks operating in space, where the latter boundary conditions are more appropriate.

We also evaluated the effect of increasing the cutoff frequency f_{max} on the behavior of the eigenfrequency counting function $N'(f)$ obtained from data. Figure 7 shows a further comparison for the case of $f_{max} = 3$ kHz. One can see that above 1.8 kHz the experimental and theoretical eigenfrequency counting functions begin to diverge, and the experimental curve fails to capture the high-frequency asymptotics of the spectrum due to insufficient peak resolution. As a consequence, the predicted value of the volume from the above procedure no longer agrees with the actual value. This indicates that the individual peak resolution is a crucial factor in determining the accuracy of the proposed mass gauging method.

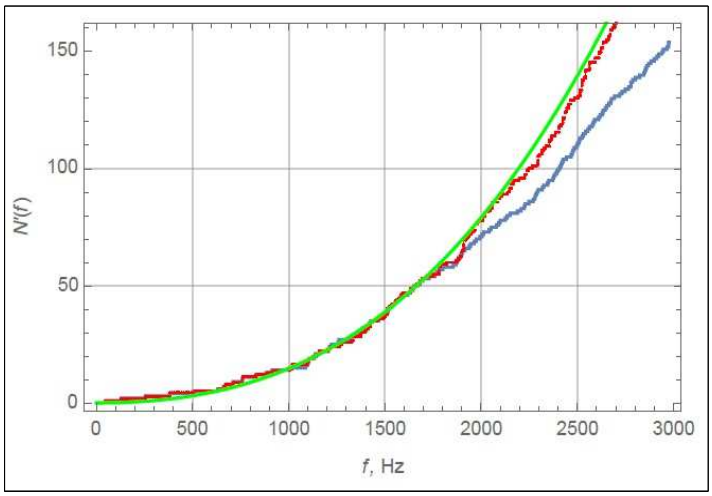

Figure 7. The eigenfrequency counting function $N'(f)$ obtained from theory (red), experimental data (blue) and Weyl's asymptotic formula (green) for the large Dewar tank in Fig. 5 with the cutoff frequency $f_{max} = 3$ kHz.

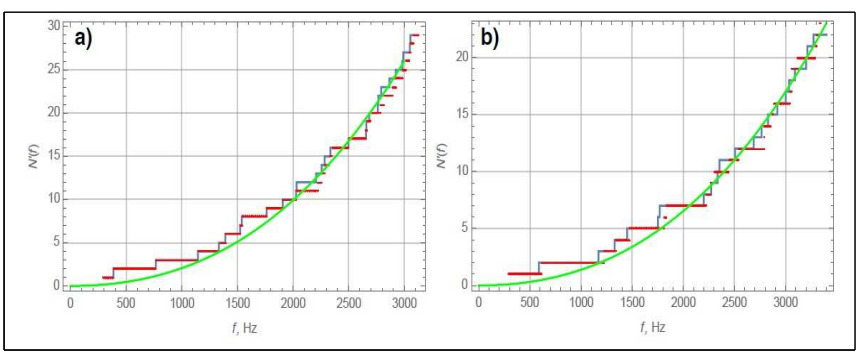

Figure 8. The eigenfrequency counting function $N'(f)$ obtained from theory (red), experimental data (blue) and Weyl's asymptotic formula (green) for the smaller cylindrical tank with $R = 7.5$ cm and $H = 45$ cm, using the cutoff frequency $f_{max} = 3$ kHz. In (a), the results for an empty tank (ullage volume 8 liters) are shown. In (b), the results for a partially filled tank (ullage volume 5 liters) are shown.

We have also carried out our volume estimation procedure for a cylinder partially filled with water to different levels. A smaller cylinder was used for these tests, with $R = 7.5$ cm and $H = 45$ cm. The total volume of this cylinder is about 8 liters. Measurements were carried out for an empty (air-filled) cylinder and for the cylinder filled with 3 liters of water at the bottom. Two data sets corresponding to different tap locations and the cutoff frequency of $f_{max} = 3.4$ kHz were used to reliably detect about 30 frequency peaks. Further increase in the value of f_{max} did not produce any improvements. The results of the comparisons between the theoretical predictions and the observations are shown in Fig. 8. Once again, there is an excellent agreement for the entire spectral interval on which the eigenfrequencies were reliably detected. Fitting the empty tank data to Eq. (35) yields $A' = 4.06287 \times 10^{-10}$ s^3 and $B' = 1.56373 \times 10^{-6}$ s^2, resulting in the prediction of the volume by Eq. (36) to within 2% uncertainty. The theoretical spectrum on this spectral interval yields the volume with the uncertainty of 5%. Similarly, in the case of the partially filled cylinder we obtained $A' = 2.17452 \times 10^{-10}$ s^3 and $B' = 1.22988 \times 10^{-6}$ s^2, yielding the ullage volume to within 15% uncertainty. The theoretical spectrum yields the volume prediction for this geometry that is accurate to within 11%.

4.2 Liquid modes counting tests

As our discussion in Section 3 implies, mode counting in the liquid compartment of a partially filled tank is expected to be advantageous for the volume inference for the following reasons:

- Higher resolution available in terms of N_{max};
- Lower interference (larger spectral separation) of the cavity and shell modes;
- Boundary conditions are closer to Dirichelet (pressure release) conditions, leading to faster convergence of the error with modes count number N.

Therefore, in the second series of experiments were focused on modes counting in liquid compartment. Water was used as the working fluid. A number of hardware modifications were made, Figure 9 (a). An actuation technique for the acoustic emission was developed using solenoid actuator, Figure 9 (b). The solenoid actuator was attached to the tank wall from the outside and applied a short ping to excite acoustic resonances in the liquid compartment. The detection was performed using accelerometers attached to the wall from the outside as well, Figure 9 (c). Initially, the detection was also performed with hydrophones immersed into the water. However, since accelerometers proved to give sufficiently good signal, they were adopted in latter tests. Using the solenoids and

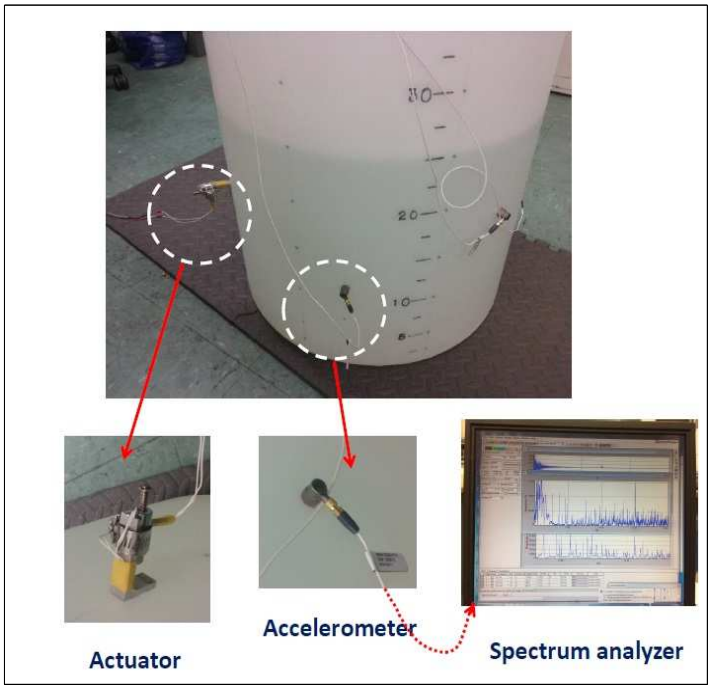

Figure 9. Hardware used for liquid modes counting.

Figure 10. The 200-liter tank used in liquid modes counting tests.

accelerometers mounted on the wall from the outside makes the excitation/detection technique nonintrusive which is a very significant advantage for propellant volume gauging applications.

A 200 liter plastic tank was used, Figure 10, which adequately simulates the Dirichlet (pressure release) boundary condition expected for liquid propellants such as LOx in thin Aluminum alloy or steel tanks. Measurements were performed on both settled and unsettled, by either tilting the tanks or immersing air-filled balloons in the liquid, Figure 11. Various filling levels were used. About 10 excitations per configuration were performed at various locations on the wall, giving 10 time-series and the corresponding spectra. Each time series were recorded using 3 accelerometers and a hydrophone. Figure 12 shows spectra obtained from 10 different actuation locations on the tank wall as detected by one of the accelerometers (blue lines). Green lines show locations of the resonances calculated for ideally cylindrical configuration of the water in the tank, for the same volume and Dirichlet boundary conditions. The correspondence of the spectra is remarkable due to a relatively weak tilt. A closer look reveals substantial deviations. The most important is, of course, the splitting of degenerate peaks present in the ideally cylindrical geometry. This splitting allows counting the total number of resonances for the fit to Weyl's law. An additional observation is the presence of shell modes, which are found to localize at the lower end of the spectra.

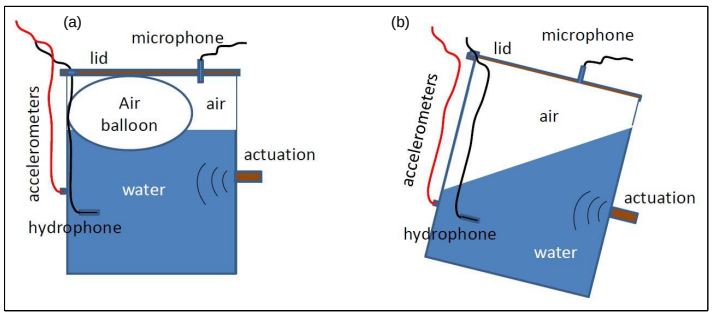

Figure 11. Representative geometries of unsettled liquid.

The effective localization of the shell modes at the lower end of the spectrum is generic and is due to their significant dissipation. Shell modes are generally much wider than the liquid resonances and don't interfere with liquid modes counting.

Peaks were counted using the information in all the spectra as it was found that particular peaks are not excited or registered for a particular location of the actuator and detector, respectively, where the mode does not couple to either actuator or detector. The counting function N(f) was compiled and fitted to Weyls law.

Figure 13 shows the mode counting results for the fill level of 100 liter and an 18 degrees tilt of the tank: the counting function $N(f)$, panel (a), the error in the inferred volume, panel (b) and the averaged error, as defined in Section 3.2, panel (c). It is found that accelerometers give similar accuracy as the hydrophone. Therefore, totally nonintrusive actuation and detection can be used. The error is seen to oscillate as observed in all the model calculations, panel (b). Averaging over the oscillations produces the average error of $< 3\%$ for the volume estimation.

The data are compared to theoretical calculations for ideally cylindrical shape of water in the absence of the tilt. Since 18 degrees is a small perturbation of the water shape the counting function is expected to be slightly perturbed compared to the ideal case. Panel (a)shows that this is indeed the case, while the fit to Weyl's law in the tilted case is excellent and distinguishable from the ideal case. It should be noted that while the counting function is only slightly perturbed by the tilt, the spectrum is perturbed substantially, as mentioned above, in the sense that the perturbation lifts the degeneracy present in the ideally cylindrical case, allowing one to count the total number of modes. We also note that the variation of the error with the upper cut-off, Figure 13 (b), is also significantly affected by the perturbation. Similar results were obtained with immersing air-filled balloons, although with a somewhat lower accuracy due to the technical challenges of immersing the balloons.

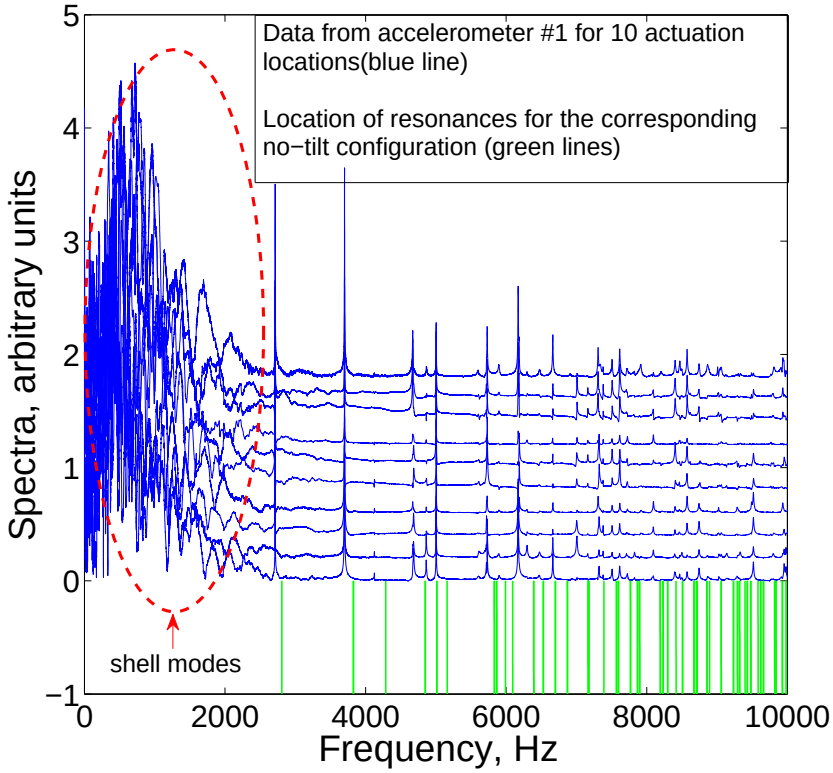

Figure 12. Spectra from accelerometer 1, excited from 10 different actuation locations on the wall (blue lines). Theoretical location of peaks for ideal cylindrical configuration of water (i.e., no tilt), corresponding to the same volume (green lines). Shell modes are seen to have no interference with the liquid modes.

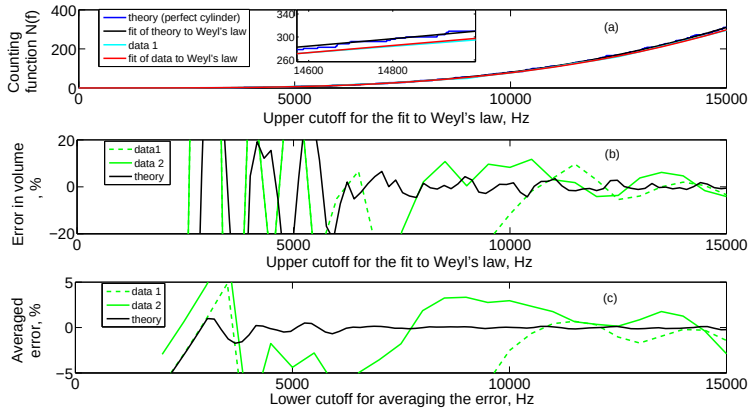

Figure 13. 100 liters of water in the tank from Figure 10, tilted by 18 degrees. 10 excitations locations have been used on the wall. Data 1 corresponds to detection by the hydrophone. Data 2 corresponds to detection by three accelerometers. Theory corresponds to ideally cylindrical shape of water in the absence of the tilt.

5 Summary and outlook

To summarize, we have presented the results of our ongoing work on the spectral mass gauging approach that uses the mathematically rigorous results about the high-frequency asymptotics of the acoustic eigenfrequencies to determine the ullage or propellant volume in a propellant tank. To this end, we considered two basic tank geometries that are most commonly used in spacecraft, namely, the cylindrical and the spherical geometries. On the theoretical side, we have carried out the analysis of the exact eigenfrequency behavior from the known explicit solutions of the Helmholtz equation for an acoustic cavity to assess the best possible performance of the method for perfect data sets. We also developed a new mass gauging principle that is applicable to settled propellant in an axially symmetric tank which uses only the axially symmetric eigenmodes. In addition, we assessed convergence properties of the error in volume inference with the counting number, the contribution and scaling of the effect of dissipation on the resolution of the peaks and the role of the tank shell modes for the quality of the volume predictions. It is predicted that convergence is significantly slower for very large or small aspect ratios of the acoustic cavity (ullage or propellant body). Peak resolution increases with the size of the tank for similar propellant configurations and is generically significantly better for liquids than for gases. The shell modes are not expected to interfere with the volume estimation in the limit of high counting number.

On the experimental side, in the first series of experiments we have performed measurements of the acoustic spectra in the ullage, using an impulse force hammer and a microphone located in the ullage for a number of tank configurations both with and without the liquid present. We developed eigenfrequency extraction and processing algorithms and ran comparisons between the predictions of our mass gauging technique and the actual ullage volumes. Using the new axial method, we were able to predict the ullage volume to within 1% solely from the acoustic measurement data for an empty sphere. We were also able to predict the ullage volume for a partially filled sphere and cylinder to within 10%–20%.

In the second series of experiments we performed mode counting of liquid (water) in partially filled tanks for a variety of unsettled configurations and filling levels. An actuation technique has been developed using solenoids mounted on the exterior of the tank wall. Accelerometers mounted on the exterior wall were used for detection of the acoustic resonances, compared to hydrophones in terms of the accuracy of the volume inference and found to perform equally well or better. As a consequence, a completely nonintrusive technique has been developed for liquid modes counting, which has significant advantages for the propellant volume gauging in-space applications. Using this technique for liquid (water) gauging in large 200 liter plastic tanks an uncertainty of $\sim 3\%$ has been achieved for "unsettled" configurations created with a tilt.

These results are encouraging, but more theoretical and experimental work is needed:

- to understand better the convergence properties of the error with the counting number;
- to assess limitation on the resolution for propellant due to temperature inhomogeneity away from thermal equilibrium;
- to assess sensitivity of the mass gauging to acoustic noise and to slosh;
- to optimize the location of actuators and detectors and the actuation protocols;
- to develop software which allows the peak counting in real time for flight applications;
- to develop and test hardware applicable for cryogenic applications and for flight-certified tanks.

References

1. M. L. Meyer, D. J. Chato, D. W. Plachta, G. A. Zimmerli, S. J. Barsi, N. T. Van Dresar, and J. P. Moder. Mastering cryogenic propellants. *J. Aerosp. Eng.*, 26:343–351, 2013.

2. F. T. Dodge. Propellant mass gauging: Database of vehicle applications and research and development studies. Technical Report CR-2008-215281, NASA, 2008.

3. C. B. Muratov, V. V. Osipov, and V. Smelyanskiy. Issues of long-term cryogenic propellant storage in microgravity. Technical report, NASA TM-2011-215988, 2011.

4. M. S. Haberbusch, B. J. Lawless, J. C. Ickes, and L. K. Walls. Reduced gravity cryotracker system. In *47th AIAA Aerospace Sciences Meeting, Orlando, FL*, AIAA Paper 2009-1599, 2009.

5. Fiber optic sensing systems for launch vehicles project. http://techport.nasa.gov/view/14652, 2015.

6. G. A. Zimmerli, K. R. Vaden, M. D. Herlacher, D. A. Buchanan, and N. T. Van Dresar. Radio frequency mass gauging of propellants. Technical Report TM-2007-214907, NASA, 2006.

7. G. A. Zimmerli, M. Asipauskas, J. D. Wagner, and J. C. Follo. Propellant quantity gauging using the radio frequency mass gauge. In *49th AIAA Aerospace Sciences Meeting*, Orlando, FL, January 2011.

8. K. M. Crosby, R. Werlink, S. Mathe, and K. Lubick. Modal evaluation of fluid volume in spacecraft propellant tanks (Proceeding Abstract). In *Annual Meeting of the Lunar Exploration Analysis Group*, October 22-24, 2012, Greenbelt, MD.

9. K. M. Crosby,T. Rundle, K. LeCaptain, and R. Werlink. Modal propellant gauging in low gravity. In *AIAA SPACE 2016*, 13 - 16 September 2016, Long Beach, California.

10. Anonymous. Propellant quantity gauging system under zero-g. Technical Report CR-119935, NASA, 1971.

11. M. H. Protter. Can one hear the shape of a drum? Revisited. *SIAM Rev.*, 29:185–197, 1987.

12. O. Giraud and K. Thas. Hearing shapes of drums: Mathematical and physical aspects of isospectrality. *Rev. Mod. Phys.*, 82:2213–2255, 2010.

13. C. Gordon, D. Webb, and S. Wolpert. Isospectral plane domains and surfaces via Riemannian orbifolds. *Invent. Math.*, 110:1–22, 1992.

14. M. Kac. Can one hear the shape of a drum? *Amer. Math. Monthly*, 73:1–23, 1966.

15. L. Borcea. Electrical impedance tomography. *Inverse Problems*, 18:R99–R136, 2002.

16. H. Weyl. Über die asymptotische verteilung der Eigenwerte. *Gott. Nach.*, pages 110–117, 1911.

17. H. Weyl. Das asymptotische Verteilungsgesetz der Eigenwerte linearer partieller Differentialgleichungen (mit einer Anwendung auf die Theorie der Hohlraumstrahlung). *Math. Ann.*, 71:441–479, 1912.

18. H. Weyl. Über die Randwertaufgabe der Strahlungstheorie und asymptotische Spektralgeometrie. *J. Reine Angew. Math.*, 143:177–202, 1913.

19. W. Arendt, R. Nittka, W. Peter, and F. Steiner. Weyl's law: Spectral properties of the Laplacian in mathematics and physics. In W. Arendt and W. P. Schleich, editors, *Mathematical Analysis of Evolution, Information, and Complexity.* Wiley-VCH, Weinheim, 2009.

20. M. Bronstein and V. Ivrii. Sharp spectral asymptotics for operators with irregular coefficients. I. Pushing the limits. *Comm. Partial Differential Equations*, 28:83–102, 2003.

21. L. D. Landau and E. M. Lifshits. *Course of Theoretical Physics*, volume 6. Pergamon Press, London, 1987.

22. C. H. Warren and A. R. Barbin. Vibration of pressurized cylinders. Technical Report DE-OC-86-16, US Army Missle Command, 1988.

23. NASA-TM-X-881. *Apollo Systems Description. Volume II. Saturn Launch Vehicles*, 1964.

24. V. Ja. Ivrii. The second term of the spectral asymptotics for a Laplace-Beltrami operator on manifolds with boundary. *Functional Anal. Appl.*, 14:98–106, 1980.

25. R. Melrose. Weyl's conjecture for manifolds with concave boundary. *Proc. Sympos. Pure Math.*, 36:257–274, 1980.

26. R. Courant. Über die Eigenwerte bei den Differentialgleichungen der mathematischen Physik. *Math. Z.*, 7:1–57, 1920.

27. B. M. Levitan. On a theorem of H. Weyl. *Doklady Akad. Nauk SSSR (N.S.)*, 82:673–676, 1952.

28. J. J. Duistermaat and V. W. Guillemin. The spectrum of positive elliptic operators and periodic bicharacteristics. *Invent. Math.*, 29:39–79, 1975.

29. R. Seeley. A sharp asymptotic remainder estimate for the eigenvalues of the Laplacian in a domain of $\mathbf{R}^3$. *Adv. in Math.*, 29:244–269, 1978.

30. E. Akhmetgaliyev, O. P. Bruno, and N. Nigam. A boundary integral algorithm for the Laplace Dirichlet-Neumann mixed eigenvalue problem. *J. Comput. Phys.*, 298:1–28, 2015.

Appendix A

Spherical geometry: theory and experiments

We now describe the experimental results that were obtained in the case of a 4 mm-thick spherical titanium tank of inner radius $R = 20.5$ cm, either empty or partially filled with water, and compare them with theoretical predictions. We note that the spherical geometry presents a rather special situation in terms of the spectral asymptotics, since in the case of the empty tank most of the eigenmodes are highly degenerate. Furthermore, an excitation by a point source at the boundary in an empty tank necessarily produces an acoustic field that is axially symmetric with respect to the line connecting the center of the sphere and the tapping location. Therefore, to compare the test results with theory, we consider only the axial modes, as was done in Sec. B in the case of a cylinder.

The theoretical spectrum for an empty spherical tank is obtained by taking $p_l = p_l(\rho, \vartheta, \varphi)$, where $(\rho, \vartheta, \varphi)$ are the spherical coordinates, and carrying out separation of variables. This leads to the eigenmodes $p_{kn}(\rho, \vartheta) = j_k(s_{kn}\rho/R)P_k(\cos\vartheta)$, where $k = 0, 1, 2, \ldots$, $n = 1, 2, \ldots$, $j_k(x)$ are the spherical Bessel functions of the first kind, s_{kn} is the n-th zero of $j_k'(x)$, and $P_k(x)$ are the Legendre polynomials. The corresponding eigenvalues equal

$$f_{kn} = \frac{c s_{kn}}{2\pi R}. \tag{A1}$$

The eigenfrequency counting function is given by Eq. (B5).

To derive the heigh-frequency asymptotics for the eigenfrequencies of both the empty tank and of the partially filled tank, we follow the arguments in Sec. B and rewrite the Helmholtz equation for the eigenmodes in cylindrical coordinates. This yields Eq. (B2), now posed in the domain

$$\Omega_0 = \left\{ (r, z) \ : \ H < z < R, \ 0 < r < \sqrt{R^2 - z^2} \right\}, \tag{A2}$$

with Neumann boundary conditions for both the rigid wall and the liquid/gas interface. Here H is the liquid fill level relative to the sphere's center. The high-frequency asymptotics is then determined by the highest-order differential operator in the left-hand side on the domain Ω_0. Thus, we are lead to Eq. (5), which takes the form

$$N_0(f) = \frac{\pi f^2}{4c^2}\left(\pi R^2 - 2H\sqrt{R^2 - H^2} - 2R^2 \arctan\frac{H}{\sqrt{R^2 - H^2}}\right) + \frac{fR}{2c}\arccos\frac{H}{R} + o(f), \qquad f \to \infty, \tag{A3}$$

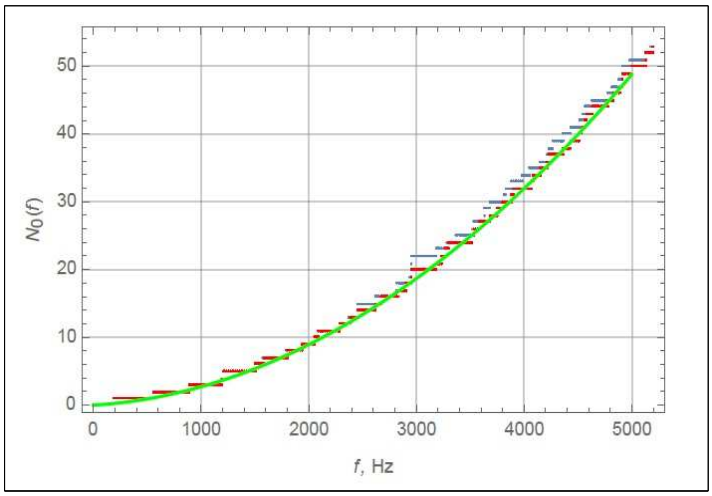

Figure A1. The eigenfrequency counting function $N_0(f)$ obtained from theory (red), experimental data (blue) and the asymptotic formula in Eq. (A5) (green) for an empty sphere of radius $R = 20.5$ cm, using the cutoff frequency $f_{max} = 5$ kHz.

where we used the explicit expressions for $|\Omega_0|$ and $|\partial\Omega_0|$ obtained from the geometry of the problem. We also note the expression for the ullage volume in the form of a spherical cap bounded by the plane $z = H$:

$$V(H) = \frac{\pi H^3}{3} - \pi H R^2 + \frac{2\pi R^3}{3}. \tag{A4}$$

The $O(f)$ term in Eq. (A3) comes from the Neumann-type contribution proportional to the perimeter of the boundary of Ω_0. This was confirmed by fitting the exact eigenvalues in the case of the empty tank to the functional form in Eq. (A3). We note that the formula in Eq. (A3) appears to be a new result in the asymptotics for an eigenvalue problem involving a degenerate elliptic operator in divergence form. Further analysis is needed to establish this asymptotic formula rigorously in a general setting.

We now turn to the comparison with the data. We begin by considering the case of an empty sphere. In this case the counting function asymptotics for the axial eigenmodes in Eq. (A3) reads

$$N_0^{empty}(f) = \frac{\pi^2 R^2 f^2}{2c^2} + \frac{\pi R f}{2c} + o(f), \qquad f \to \infty. \tag{A5}$$

We compared this formula with the measured and theoretical spectra on the spectral interval $0 \le f \le f_{max}$ with $f_{max} = 5$ kHz, capturing the first

Table A1. A comparison of the predicted liquid volumes with the actual ones ones inside the sphere of inner radius $R = 20.5$ cm. The total volume of the sphere is 36 liters.

V_{actual}, liters	$V_{predicted}$, liters	uncertainty	full-scale error
10	10.4	4 %	1%
15	19.5	30 %	13 %
20	22.7	14%	8 %
25	30.8	23 %	16%
30	26.0	13 %	11%

50 eigenfrequencies reliably. Figure A1 shows the eigenfrequency counting function obtained from data (blue), theory (red) and the asymptotics (green). We also fit the experimental data to the functional form in Eq. (B7) to obtain $A_0 = 1.74999 \times 10^{-6}$ s^2 and $B_0 = 0.00134361$ s. From these numbers, one could predict the value of the sphere radius R via the formula

$$R \simeq \frac{c\sqrt{2A_0}}{\pi}. \tag{A6}$$

The fit above reproduces the radius of the sphere to within 0.5% from the measured eigenfrequencies. The prediction from the theoretical spectrum given by Eq. (A1) is within 1.2% of the exact value. This is currently the best result that we were able to obtain from the measured data and indicates the feasibility of the proposed mass gauging approach to yield a 1% uncertainty.

We then considered the predictions of Eq. (A3) in the case of a partially filled sphere. More precisely, we fitted the eigenfrequency counting function $N_0(f)$ to the functional form in Eq. (B7) on the same frequency interval as for the empty sphere. Then, we solved for the value of H by equating the $O(f^2)$ terms in Eq. (A3) and Eq. (B7). A comparison of the mass gauging predictions with the known amounts of water in each experiment is presented in Table A1. The agreement appears to be fairly satisfactory. However, the accuracy turns out to be considerably lower than that for an empty sphere. This may be due to the excitation and detection of the shell modes and some of the non-axial eigenmodes because of either off-center tapping or off-center microphone location. Also, the prediction appears to be rather sensitive to the parameters of the algorithm used to extract the peaks. Further work is needed to make the procedure more accurate and reliable. Nevertheless, the results in Table A1 are encouraging, since they demonstrate the feasibility of our mass gauging approach at varying fill levels.

Appendix B

Axially-symmetric modes

In the cylindrical geometry, it should also be possible to excite only a small subset of the eigenmodes by taking advantage of the symmetry of the cavity. For example, one can restrict the spectrum only to the axial modes, which correspond to $m = 0$ in Eq. (11). This leads to the following set of eigenfrequencies:

$$f_{kn} = \frac{c}{2\pi}\sqrt{\frac{\pi^2(2k+1)^2}{4H^2} + \frac{a_{0n}^2}{R^2}}. \tag{B1}$$

obtained from Eq. (11) by setting $m = 0$. The corresponding eigenmodes solve

$$-\frac{\partial^2 p_{kn}}{\partial r^2} - \frac{1}{r}\frac{\partial p_{kn}}{\partial r} - \frac{\partial^2 p_{kn}}{\partial z^2} = \left(\frac{2\pi f_{kn}}{c}\right)^2 p_{kn}, \tag{B2}$$

for $k = 0, 1, 2, \ldots$, and $n = 1, 2, \ldots$, in a two-dimensional domain

$$\Omega_0 = \{(r, z) \ : \ 0 < r < R, \ 0 < z < H\}, \tag{B3}$$

with boundary conditions

$$\left.\frac{\partial p_l}{\partial z}\right|_{z=0} = 0, \quad p_l|_{z=H} = p_l|_{r=R} = 0. \tag{B4}$$

By analogy with Eq. (5), we expect that the high-frequency asymptotics of

$$N_0(f) = \sum_{k=0}^{\infty}\sum_{n=1}^{\infty}\theta(f - f_{kn}) \tag{B5}$$

is given by that of the operator with only the highest-order derivatives kept in Eq. (B2). Therefore, for the above problem we have from Eq. (5) (see also [20]):

$$N_0(f) = \frac{\pi R H f^2}{c^2} - \frac{Hf}{2c} + o(f), \qquad f \to \infty. \tag{B6}$$

The comparison of the exact expression from Eq. (B5) and its asymptotic approximation from Eq. (B6) is shown in Fig. B1. From this figure, one can see once again an excellent agreement, even for the first 40 eigenfrequencies. Also, fitting the exact expression in Eq. (B5) to the form

$$N_0(f) \simeq A_0 f^2 + B_0 f, \tag{B7}$$

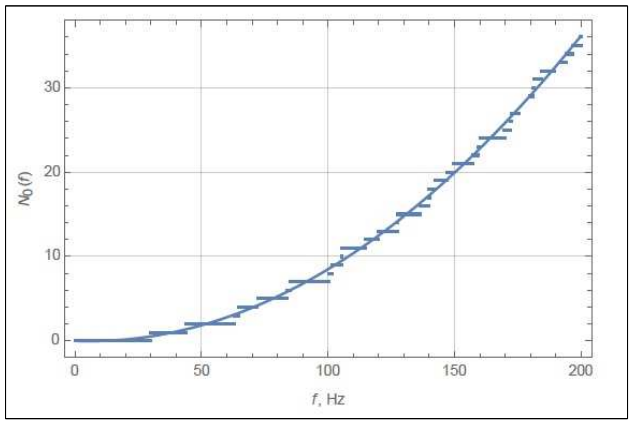

Figure B1. The eigenfrequency counting function for the ullage modes obtained from Eq. (B5) (broken line) and from Eq. (B6) (solid line).

and setting

$$H \simeq \frac{c^2 A}{\pi R}, \tag{B8}$$

we can obtain the height of the ullage from the fitted value of A_0. With this procedure applied on the spectral interval $0 \leq f \leq f_{max}$ with $f_{max} =$ 200 Hz, we were able to recover the exact value of H to within 2.5% uncertainty. This indicates that using the axially-symmetric part of the spectrum may be also a very efficient way of measuring the level of settled or partially settled propellant in a cylindrical tank.

REPORT DOCUMENTATION PAGE

Form Approved
OMB No. 0704–0188

The public reporting burden for this collection of information is estimated to average 1 hour per response, including the time for reviewing instructions, searching existing data sources, gathering and maintaining the data needed, and completing and reviewing the collection of information. Send comments regarding this burden estimate or any other aspect of this collection of information, including suggestions for reducing this burden, to Department of Defense, Washington Headquarters Services, Directorate for Information Operations and Reports (0704-0188), 1215 Jefferson Davis Highway, Suite 1204, Arlington, VA 22202-4302. Respondents should be aware that notwithstanding any other provision of law, no person shall be subject to any penalty for failing to comply with a collection of information if it does not display a currently valid OMB control number.
PLEASE DO NOT RETURN YOUR FORM TO THE ABOVE ADDRESS.

1. REPORT DATE *(DD-MM-YYYY)*
01-01-2018

2. REPORT TYPE
Technical Memorandum

3. DATES COVERED *(From - To)*
10/2015–9/2016

4. TITLE AND SUBTITLE
Spectral mass gauging of unsettled liquid with acoustic waves

5a. CONTRACT NUMBER
NNA14AA60C

5b. GRANT NUMBER

5c. PROGRAM ELEMENT NUMBER

6. AUTHOR(S)
Jeffrey Feller, Ali Kashani, Michael Khasin, Cyrill Muratov, Viatcheslav Osipov and Surendra Sharma

5d. PROJECT NUMBER

5e. TASK NUMBER

5f. WORK UNIT NUMBER
WBS: 295670.01.02.91

7. PERFORMING ORGANIZATION NAME(S) AND ADDRESS(ES)
NASA Ames Research Center, Moffett Field, CA, 94035-0001

8. PERFORMING ORGANIZATION REPORT NUMBER
xxxxx

9. SPONSORING/MONITORING AGENCY NAME(S) AND ADDRESS(ES)
National Aeronautics and Space Administration
Washington, DC 20546-0001

10. SPONSOR/MONITOR'S ACRONYM(S)
NASA

11. SPONSOR/MONITOR'S REPORT NUMBER(S)
NASA/TM–2018–219876

12. DISTRIBUTION/AVAILABILITY STATEMENT
Unclassified-Unlimited
Subject Category 28
Availability: NASA CASI (443) 757-5802

13. SUPPLEMENTARY NOTES
An electronic version can be found at http://ntrs.nasa.gov.

14. ABSTRACT

Propellant mass gauging is one of the key technologies required to enable the next step in NASA's space exploration program. At present, there is no reliable method to accurately measure the amount of unsettled liquid propellant of an unknown configuration in a propellant tank in micro- or zero gravity. We propose a new approach to use sound waves to probe the resonance frequencies of the two-phase liquid-gas mixture and take advantage of the mathematical properties of the high frequency spectral asymptotics to determine the volume fraction of the tank filled with liquid. We report the current progress in exploring the feasibility of this approach, both experimental and theoretical. Excitation and detection procedures using solenoids for excitation and both hydrophones and accelerometers for detection have been developed. A $\sim 3\%$ uncertainty for mass-gauging was demonstrated for a 200-liter tank partially filled with water for various unsettled configurations, such as tilts and artificial ullages. A new theoretical formula for the counting function associated with axially symmetric modes was derived. Scaling analysis of the approach has been performed to predict an adequate performance for in-space applications.

15. SUBJECT TERMS
mass-gauging, micro-gravity, zero-gravity, acoustic waves, spectral theory

16. SECURITY CLASSIFICATION OF:			17. LIMITATION OF ABSTRACT	18. NUMBER OF PAGES	19a. NAME OF RESPONSIBLE PERSON
a. REPORT	b. ABSTRACT	c. THIS PAGE			STI Help Desk (email: `help@sti.nasa.gov`)
U	U	U	UU	40	19b. TELEPHONE NUMBER *(Include area code)* (443) 757-5802